Development and application of a point Doppler velocimeter featuring two-beam multiplexing for time-resolved measurements of high speed flow

Tobias Ecker[1], Donald R. Brooks[1], K. Todd Lowe[1] and Wing F. Ng[2]

[1]*Department of Aerospace and Ocean Engineering,*
[2]*Department of Mechanical Engineering*
Virginia Tech, Blacksburg, VA 24061

Abstract
A novel point Doppler velocimeter (pDV) based upon the Doppler Global velocimetry (DGV) principle is presented which is capable of three-component velocity vector measurements at 100 kHz mean rates over extended time periods. In this implementation two laser beams are multiplexed to illuminate the flow over alternating time windows, providing for a reduction in the number of sensors required. The implications of this multiplexing paradigm coupled with the fundamental limits set by the optical absorption filter are examined in detail and uncertainties are predicted via instrumentation modeling and representative synthetic flow data. The results indicate that the multiplexing pDV instrument provides the required temporal and velocity resolution for turbulent shear flows at velocities of nominally 500 m/s. As a demonstration and validation of this time-resolved technique, statistics of three-velocity component measurements in a cold, supersonic, over-expanded jet at jet exit Mach number M_j=1.4 (Design Mach number M_d=1.65) are presented. Time resolution up to 250kHz and instantaneous velocity uncertainties between 6.6 and 11.1 m/s were obtained. Comparisons of mean pDV data with laser-Doppler velocimetry (LDV) data are consistent with uncertainty predictions for the technique. The ultimate value of the instrument is exhibited in the analysis of Reynolds stress spectra in the screeching jet, exposing the spatial development of motions at the harmonics of the screech tone, variable phase coordinated shock motions, and growth of turbulent fluctuations in the developing shear layer of the jet. From the data presented the screech tone phenomenon is suspected to be linked to the production of radial-azimuthal shear stresses in extended regions beyond the potential core.

Keywords: time-resolved velocimetry, Doppler Global Velocimetry, supersonic jet, jet noise

1. Introduction

Particle-based velocimetry techniques have been developing towards time-resolved capabilities over the last decade, shedding insight into the complex physics of unsteady fluid dynamics and turbulent phenomena and their associated time scales.

Doppler global velocimetry (DGV) is an optical, non-intrusive, particle scattering based velocimetry technique utilizing the absorption characteristics of molecular gas cells. In its essence it was developed in 1990 by Komine (1990) and matured by Komine et al. (1991) as well as Meyers and Komine (1991) as a planar alternative to particle image velocimetry (PIV) particularly well suited for high speed flows due to its absolute uncertainties. Compared to laser Doppler velocimetry (LDV), DGV has the potential of a higher temporal response, as it does not require resolution of signals from single particles. As multiple particles may contribute to the Doppler signal, sufficiently high concentrations of very small particles may produce continuous datasets with minimal particle lag.

In this study we describe the development of a point Doppler velocimeter (pDV) based on the DGV principle and capable of time-resolved measurement in high-speed flows. A distinctive feature of this development, aside from the high data rate is the use of a time-shift multiplexing technique to generate time-resolved 3 component velocity vectors with a reduced number of required sensors. Detailed studies on the errors due to the time shift multiplexing and its data processing technique are presented along with a study on systematic and random uncertainties. Additionally the influence of the absorption line width on velocity statistics is used to determine instrument capabilities and limitations. At the end of this study the real world applicability of the pDV sensor is demonstrated with measurements in a cold supersonic jet generated by a biconic nozzle with design Mach number (M_d) of 1.65. The acousto-optic beam multiplexing technique enables measurements of velocity vectors at 100 kHz mean rates over extended time windows. Validation measurements performed at different nozzle-pressure ratios (NPR) are compared

with measurements from a LDV probe. Measurements in a supersonic jet operated at over-expanded and screeching condition (total temperature ratio, TTR = T_0/T_a =1; T_0, total temperature; T_a, ambient temperature; NPR=3.2; jet exit Mach number, M_j=1.4) are used to generate auto-correlations, auto-spectra, mean velocity as well as normal and shear stress information along the streamwise coordinate. The results indicate fundamental structural differences between over and under-expanded jet screech and a link between screech and shear stress production in downstream regions.

1.1 State of the Art

DGV is a particle scattering technique based on the frequency dependent absorption characteristics of molecular gas cells resulting in direct measurement of the Doppler effect. Meyers et al. (2001) summarize the efforts to characterize the sources of uncertainty in DGV. The main sources of uncertainty are attributed to the molecular gas cell, laser stability and characteristic performance and configuration of the sensor type.

There have been several notable developments of the DGV technique over the past decade. Advances have been made to address one of three goals: measurement uncertainty reduction, reduction of instrumentation cost and complexity, as well as time resolution. Elliot and Beutner (1999) presented a major contribution to the characterization and reduction of DGV uncertainty for several applications. One of the key developments presented therein was the use of vapor limited gas absorption cells that reduces the errors incurred due to temperature variations in the cell.

There are several efforts reported in the literature to reduce the cost and complexity of DGV by reducing number of detectors. Charret et al. (2004) introduced the two-frequency DGV ($2\nu DGV$) approach to eliminate the reference sensor and its associated uncertainties. In this approach an Acousto-optic modulator (AOM) is used to shift the laser line to a frequency with very little absorption by the molecular gas filter. The signal obtained at this frequency is then used as a reference, enabling one detector per velocity component, further reducing equipment cost and measurement uncertainty due to beamsplitting arrangements and sensor gain. Another technique, frequency modulated DGV (FM-DGV) first introduced by Mueller et al. (1999) reduces the required number of sensors and associated beam splitting uncertainties by evaluation of first and second order harmonics of the resulting amplitude modulation. Other approaches to sensor reduction is the use of fiberoptic bundles to project several fields of view onto the same sensor (Nobes et al. 2004) or a laser frequency scanning technique combined with cross correlation processing as recently applied by Cadel et al. (2014a,b).

The development of time resolution techniques for DGV has included several contributions, from optimization of flow-freezing instantaneous measurements to high repetition rates. The first instantaneous measurements in supersonic flow in which the capability to generate velocity vectors that froze the flow at the smallest time scales were first demonstrated by Smith (1998) and Clancy et al. (1999). The ability to provide high repetition measurements came primarily with the development of detector, laser and data acquisition technologies capable of sampling at these high rates. The pDV technique concentrates the laser energy onto a small measurement volume, therefore improving signal to noise ratios in an effort of high accuracy and ideally time-resolved data. First efforts were presented by Kuhlman et al. (2001) on the application to turbulent jet flows and instrument uncertainty characterization. The one-component pDV system presented by Cavone et al. (2006) demonstrates first time-resolved measurements similar to LDV at frequencies up to 20 kHz. The FM-DGV technique already mentioned has been demonstrated at points and with arrays of detectors (Müller et al. 1999; Fischer et al. 2008; Fischer et al. 2010). Fischer et al. (2007; 2008) reported the uncertainty of the FM-DGV technique to be as low as 0.02 m/s. Current developments show approaches to time resolution to up to 100 kHz for one velocity component (Fischer et al. 2008) and 20 kHz for 3-component probes (Fischer et al. 2011). Thurow et al. (2005) demonstrated the application of a one-component, high repetition rate DGV system based on a high-speed camera (128 x 64 pixels) in a rectangular Mach 2.0 jet - to our knowledge the first application of a high repetition rate DGV technique in a supersonic jet flow. Measurements were performed at 250 kHz frame rates but image buffer limitations constrained the recording timespan and therefore prevented the observation of flow structure evolution at integral time scales. According to our survey, true time-resolved measurements using DGV, where the time-resolved term refers to the capability of resolving all or most time scales of interest (as used by Wernet (2007) for time-resolved PIV in jets), has only been demonstrated by the FM-DGV technique (e.g., Fischer et al. 2011) and in the current work.

The article by Thurow et al. (2005) demonstrates the current trade-off between spatially and temporally resolving optical, non-intrusive measurements in high-speed flows that must to be addressed to

gain deeper understanding of the physics involved. In a first step to address these trades-off for our application in high speed jet flows, we here introduce an effort to obtain time-resolved measurements at reduced equipment complexity for a single point with a optically non-distorting configuration that allows extension to multiple points and planes in the future. In continuation of this approach Ecker et al. (2014a) presented an extension to 32 points using a newly developed Photomultiplier (PMT) camera.

1.2 Principle of Doppler Global Velocimetry

DGV relies on the detection of the Doppler shift of laser light scattered by submicron-sized particles following the local flow. A single-longitudinal-mode laser is tuned such that the Doppler shifted light scattered by particles lies within a frequency range of high transmission sensitivity for the molecular gas filter. The frequency of the scattered light is therefore transformed to a function of the intensity of light exiting the gas filter. In its classic implementation, DGV techniques utilize the ratio of filtered-to-unfiltered light intensity in a reference design to obtain Doppler shift frequencies, as done in the present work.

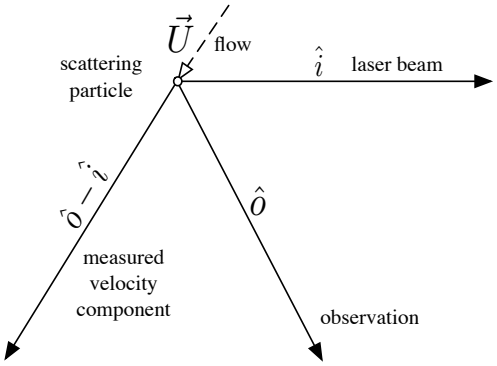

Fig. 1 Vector geometry and nomenclature of the DGV measurement principle.

The Doppler shift of scattered light depends upon the laser frequency, vector particle velocity, and laser propagation and observation directions (Meyers and Komine 1991) (see figure 1):

$$\boldsymbol{f_D = f_0 \frac{\vec{U}\cdot\vec{e}}{c}} \qquad (1)$$

where f_0 is the incident laser light frequency, $\boldsymbol{c}$ is the speed of light, $\vec{U}$ is the particle velocity vector, $\vec{e} = \hat{o} - \hat{\imath}$ defines the velocity measurement component direction, wherein the laser propagation direction is the unit vector $\hat{\imath}$ and the direction of observation is given by $\hat{o}$. With a three-component measurement, the resulting velocity vector in the coordinate system of interest may be reconstructed from the measured components and their base vectors as:

$$\vec{\boldsymbol{U}} = \begin{bmatrix} \vec{\boldsymbol{e}}_{\boldsymbol{1}}{}^{\boldsymbol{T}} \\ \vec{\boldsymbol{e}}_{\boldsymbol{2}}{}^{\boldsymbol{T}} \\ \vec{\boldsymbol{e}}_{\boldsymbol{3}}{}^{\boldsymbol{T}} \end{bmatrix}^{-1} \begin{pmatrix} \boldsymbol{u_1} \\ \boldsymbol{u_2} \\ \boldsymbol{u_3} \end{pmatrix} = \begin{bmatrix} R_{11} & R_{12} & R_{13} \\ R_{21} & R_{22} & R_{23} \\ R_{31} & R_{32} & R_{33} \end{bmatrix} \begin{pmatrix} \boldsymbol{u_1} \\ \boldsymbol{u_2} \\ \boldsymbol{u_3} \end{pmatrix} \qquad (2)$$

where $\vec{e}_i$ represents the measurement vectors and u_i the magnitude of the respective directly measured velocity component. Similarly R represents the geometrical calibration deduced for every instrument configuration.

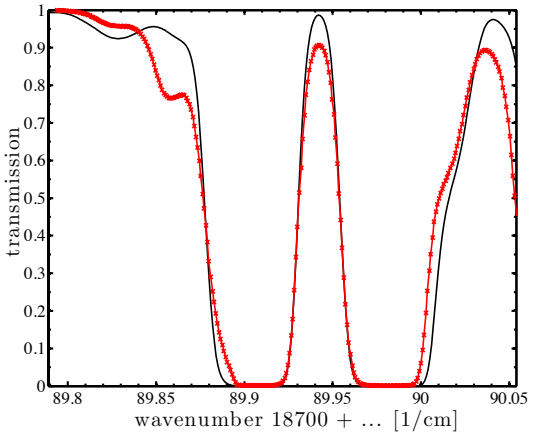

Fig. 2 Measured iodine cell scan (red) compared to model using code by Forkey (black)

The laser frequency may be tuned in steps to characterize the transmission function of the molecular gas cell as well as to choose the exact reference frequency. The calibration scan can then be converted into usable calibration data by matching the experimental scan to numerical transmission spectra based on a model developed by Forkey (1996) or by comparing it to a known frequency shift, e.g. using a calibration wheel, AOM or measurement of a known flow.

This numerical calibration scheme has been used successfully by Fischer et al. (2000), Meyers and Lee (2010) and other authors (Müller et al. 1999; Jones 2001; Fussell 2003). Figure 2 shows an experimental scan compared to the numerically obtained transmission spectrum, using model and code developed by Forkey et al. (1997). Further requirements and characteristics to the use of iodine based absorption filters for DGV can be found in in detail in Chan et al. (1995).

2. Apparatus and instrumentation

2.1 Probe design

The presented pDV sensor is based on the DGV principle and utilizes two sets of laser sending optics at the top and bottom of the device at an angle to the main flow direction. Two receiving optics assemblies collect the light from the measurement volume. This configuration can be seen in figure 3. In order to distinguish multiple velocity components with a two-receiver setup time shifted multiplexing (alternate flashing) of the two laser beams is necessary. AOMs allow sub microsecond time shift multiplexing while enabling amplitude modulation and frequency shift capabilities.

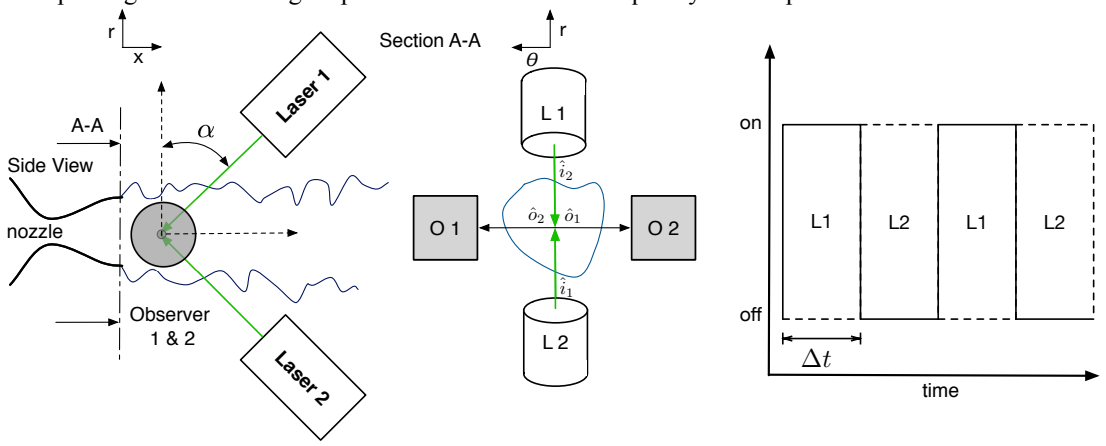

Fig. *3* Schematic of the pDV optical arrangement (O 1: Observer 1, O 2: Observer 2, L 1: Laser 1, L 2: Laser 2) (a), section view (b) and beam multiplexing (c)

While using AOMs present an extra effort and limit the smallest resolvable time scale, their application is essential to the further development of the envisioned applications of planar time-resolved measurements and eventual volumetric scanning (e.g., Lowe et al. 2012). This geometric configuration allows using planar arrays of sensors for planar vector velocity measurements with very little perspective distortion. Further, owing to the reduced perspective distortion and depth of field mitigation, the use of large aperture lenses and compatibility with depth-wise laser sheet scanning are both enabled. More details on the application of laser sheet scanning for volumetric imaging are given by Thurow and Lynch (2009).

Therefore the presented instrument is based on a quasi-instantaneous time shift technique, providing two velocity components shifted in time allowing reconstruction of a full 3-component velocity vector with a high temporal resolution. The influence of the time shift multiplexing and beam intersection angle on temporal errors and physical uncertainties will be thoroughly discussed in the following studies. Additionally the influence of turbulent fluctuations on flow statistics due to the properties of the transmission-frequency transfer function is discussed

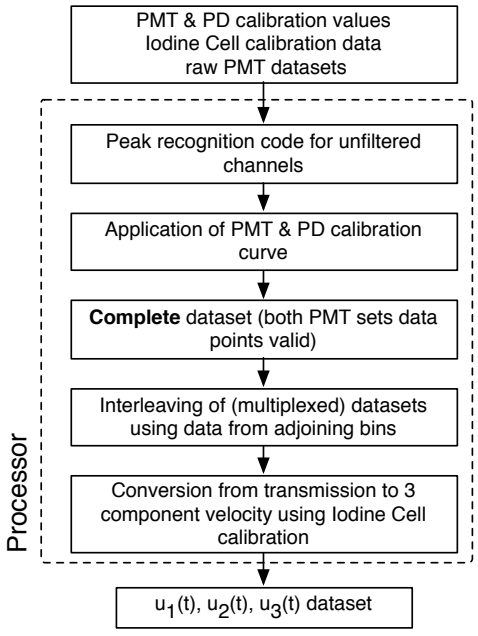

Fig. 4 Flow chart for the multiplexing data processing employed.

2.2 Signal processing

The signal processing flow is displayed step by step in figure 4. First a peak detection algorithm determines valid photon signals in both unfiltered channels separately. After applying detector calibration values, complete datasets are identified as such with valid signals present in both unfiltered channels. Due to the beam multiplexing two interleaving datasets exist and missing values are completed from the adjacent multiplexing window and the arrival time is defined as the average arrival time of both data points.

Doing so results in 4 transmission values for each time sample. The iodine cell transfer function is then applied to the measured and the known reference transmission values to determine the differential Doppler frequency. From the Doppler measurement direction vectors a rotation matrix R is created and three-component time-resolved velocity vectors in the base coordinate system determined similar to the process described by Charrett et al. (2007).

3. Method verification and performance analysis

3.1 Processing Uncertainties

In order to optimize, validate and determine uncertainty of the pDV multiplexing and data processing, a synthetic velocity signal is to a model for the instrumentation and particle sampling. The signal is constructed from a one-dimensional model turbulent power spectrum (Pope 2000) and random phase spectrum. The parameters for the model spectrum allow to include integral and Kolmogorov timescales, such that the inverse Fourier transform of the model provides realistic time-series data that may then be scaled and shifted to simulate the desired mean velocity and turbulence intensity. In order to simulate particle arrival statistics, random arrival times are generated using Poisson statistics and the final velocity dataset is obtained at the arrival times from the original oversampled signal.

Tab 1. Simulation time scales and frequencies

Time resolution	Δt
Measurement rate	Particle arrival time (250 kHz)
Sample rate	Not applicable as in practice much higher than particle transit time
Cut off frequency	$1/\tau$

The velocity and time scales were chosen to be representative of the experiments in supersonic jets. The integral timescales to be resolved for a supersonic jet flow are on the order of the shear layer thickness divided by the eddy convection velocity, which for the flows investigated is about approximately 10-30 µs (Brooks et al. 2014a). The Kolmogorov time scales η in this type of flow are much smaller and can be estimated from the DNS data of Freund et al. (2000) to be on the order of 0.5 µs at the minimum. Quasi-instantaneous techniques like PIV or the here presented time-multiplexed pDV cannot accurately resolve down to the finest scales due to temporal averaging. However as most relevant and energetic time scales are much larger, this issue loses importance. All reported errors or uncertainties are in relation to measurement of a flow resolved to a smallest timescale of interest of τ=10 µs. This constraint is realized as a high frequency cutoff at the desired timescale with zero padding up to the Nyquist frequency. Simulation time scales are explained in table 1. The turbulent kinetic energy (q) values used to generate the model signal are estimated from the prescribed turbulent intensity and the mean velocity of the flow.

$$q = I^2 U^2 \frac{3}{2}$$

where I is the turbulence intensity and U the mean velocity vector.

The dissipation rate ε is estimated from the Kolmogorov timescale (η =1 µs) and the kinematic viscosity for the flow and is about $2.5 \times 10^6 .m^2 s^{-3}$, resulting in a spectral shape similar to spectra reported by Brooks et al (2014a).

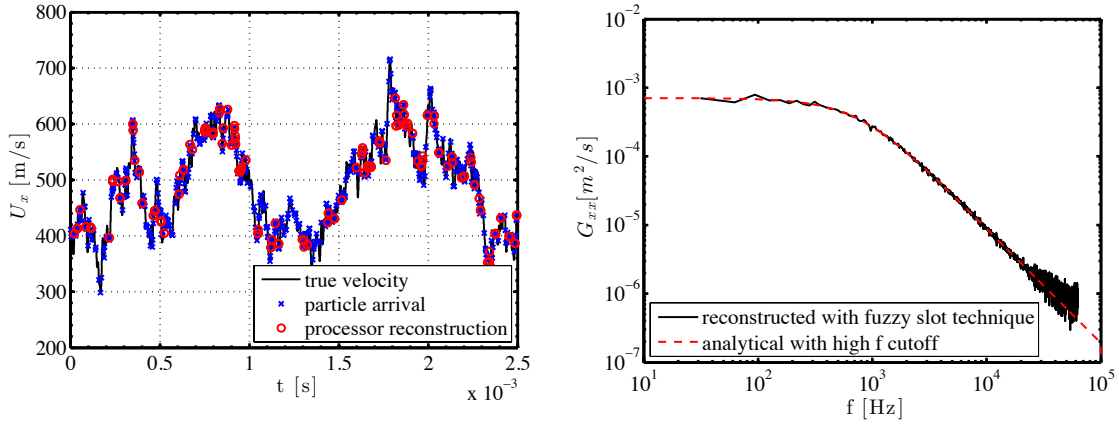

Fig. 5 Streamwise velocity reconstruction (a), streamwise velocity spectra (b), Δt=2.0 µs interval for a 500 m/s, I=0.15 example case, η =1 µs

For the purpose of the numerical uncertainty analysis of the multiplexing portion, the Doppler frequency shift is assumed to be known. When processing the synthetic data, the dataset is first attributed to the two alternating laser beams and then run trough the processor. An example of the reconstructed velocity compared to the synthetic velocity data and an example of the reconstructed spectrum are shown in figure 5. The spectral information was obtained by using a fuzzy slot correlation processing scheme as introduced by Benedict et al. (2000). All reported quantities are given in a cylindrical coordinate system with streamwise (x), radial (r) and azimuthal (Θ) components, unless otherwise noted.

As will be shown, the main contributor to the random error (the difference between the input and the recovered values) is the multiplexing time interval Δt, which is the time each beam illuminates the measurement volume before it switches to the complementing beam (compare figure 3 c). This multiplexing time effectively limits the temporal response of the instrument and influences the processing uncertainties due to temporal averaging effects. It is important to note that the processing scheme provided an un-biased mean velocity estimate for all multiplexing time intervals studied in the limit of large sample sets.

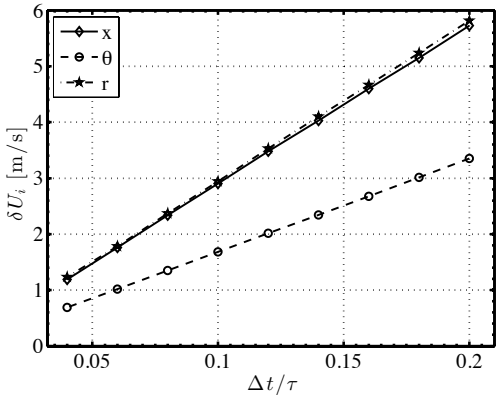

Fig. 6 RMS uncertainty estimate for instantaneous measurement due to temporal averaging

Figure 6 shows the instantaneous root mean square (RMS) uncertainties of all three components for an example case (*U=[500,30,20] m/s, I=0.15, α=45°*) at different time scale ratios. It can be seen that the error is the largest for the streamwise and radial component, but smaller for the azimuthal component. The differences in the magnitude in the components of these instantaneous velocity errors are caused by the different spatial sensitivities due to the geometric composition of the instrument measurement vectors (compare eq. 2). This dominantly absolute processing error as such scales with the nature of the flow and its associated timescales to be measured. It may be noted that for heated jets, the uncertainty would increase slightly as temporal scales decrease due to greater convective speeds

3.2 Physical Uncertainties

Each velocity component u_i (*i*=1,2,3,4) in measurement direction ($\hat{e}_i = (\hat{o} - \hat{\imath})_i$) can be described by the Doppler equation.

$$u_i = \left(\frac{f_i}{f_0} - 1\right) c \quad (3)$$

Considering the system as a transfer function $y = \mathrm{F}(x_j)$ dependent on j=1,2...,n independent variables, the sensitivity of the system can be described by the sum of linearized Taylor series of the single independent variables.

$$\delta u_i = \sqrt{\left(\frac{\partial u_i}{\partial f_i}\right)^2 (\delta f_i)^2 + \left(\frac{\partial u_i}{\partial f_0}\right)^2 (\delta f_0)^2} \quad (4)$$

$$\text{where } \frac{\partial u_i}{\partial f_i} = \frac{c}{f_0} \text{ and } \frac{\partial u_i}{\partial f_0} = -c\frac{f_i}{(f_0)^2}$$

The transfer function of the iodine cell can be simplified to a linear function, transducing the transmission *T* on the flank of a transmission line into frequency *f*. Subscript *i* denotes the measured component and subscript 0 refers to the reference state. Therefore the uncertainty in each measured component is a combination of systematic and random uncertainties, similar to the expression derived by Reinath (1997):

$$\delta u_i = \frac{c}{f_0}\sqrt{\left(\frac{df}{dT}\right)_i^2 (\delta T_i)^2 + T_i^2\left[\delta\left(\frac{df}{dT}\right)_i\right]^2 + \frac{f_i^2}{f_0^2}\left\{\left(\frac{df}{dT}\right)_0^2 (\delta T_0)^2 + T_0^2\left[\delta\left(\frac{df}{dT}\right)_0\right]^2\right\}} \quad (5)$$

Thus it can be seen that the uncertainty in this reference based DGV system is dependent on the uncertainty in the slope of the transmission line, the local transmission as well as the frequency of both the shifted and the unshifted signals. These uncertainties are directly related to the respective uncertainties for the Iodine cell calibration, in the signal to noise ratio and beam splitter transmission ratio. While the transmission uncertainty is mainly random, the uncertainty in the slope of the transmission line is systematic and will represent as bias in the experimental results. The random errors are most significant for instantaneous time resolved measurements and the derived higher order moments. The single component

uncertainty and the uncertainty in the measurement vector angles result in the uncertainty for each 3-component measurement. The total uncertainty of the measurement including the uncertainty in the geometrical calibration matrix R is represented by:

$$\Delta\vec{U} = \begin{pmatrix} \delta \boldsymbol{u_x} \\ \delta \boldsymbol{u_\theta} \\ \delta \boldsymbol{u_r} \end{pmatrix} = \sqrt{\left(\begin{bmatrix} R_{11} & R_{12} & R_{13} \\ R_{21} & R_{22} & R_{23} \\ R_{31} & R_{32} & R_{33} \end{bmatrix}\right)^2 \begin{pmatrix} \delta u_1 \\ \delta u_2 \\ \delta u_3 \end{pmatrix}^2 + \left(\begin{bmatrix} \delta R_{11} & \delta R_{12} & \delta R_{13} \\ \delta R_{21} & \delta R_{22} & \delta R_{23} \\ \delta R_{31} & \delta R_{32} & \delta R_{33} \end{bmatrix}\right)^2 \begin{pmatrix} u_1 \\ u_2 \\ u_3 \end{pmatrix}^2} \quad (6)$$

3.3 System total uncertainties

The system's uncertainties are a mixture of physical and data processing/time averaging uncertainties and errors. The error in the transmission estimate from the Doppler shifted photon bursts is estimated by conducting Monte Carlo simulations of a simple Gaussian burst signal model with Gaussian noise superimposed. The Gaussian burst envelope A(t) is modeled as:

$$A(t) = Ke^{-\frac{t^2}{2s^2}} \quad (8)$$

where $s = t_0/6$, t_0 is the particle transit time, K is a constant with units of energy [J]. Similar models have been previously used for uncertainty estimates in LDV (Ecker et al., 2012).

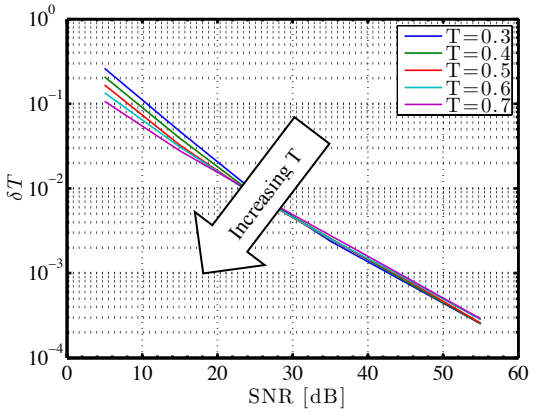

Fig. 7: Transmission error in the burst processing for different SNR

Figure 7 depicts the RMS error for each signal to noise ratio ($SNR = 10\log_{10}\left(\frac{P_{signal}}{P_{noise}}\right)$; power, P) estimated from a 100,000 bursts Monte Carlo. The SNR is based on the reference and it is assumed that noise is of equal power both for the reference as well as the shifted signal. Therefore lower transmission values result in higher errors to the transmission estimate. The uncertainty in the reference transmission is assumed to be very low as the SNR can be freely chosen by varying the reference laser power. The parameters used for the following system uncertainty estimates are summarized in table 2.

Tab. 2 Parameters used for physical uncertainty estimate

Parameter	*Uncertainty*
δT_i	*0.018*
δT_{ref}	*0.005*
$\delta\left(\frac{df}{dT}\right)$	$0.005\overline{\left(\frac{df}{dT}\right)}$

Assuming that the sources of errors analyzed here are uncorrelated, all errors may be considered by finding the resulting norm, analogous to applying equation 4. Figure 8 gives the total uncertainties due to the DGV sensitivities and data processing errors for an example case *(U=[500,30,20] m/s, I=0.15, SNR=20dB,* Δt = 2 μs*)*. As the processing error is relative small, the bias and instantaneous uncertainty are dominated by the sensitivities to the uncertainty in transmission and transmission slope as well as the geometric composition of the instrument. While the azimuthal velocity uncertainties are almost constant, the uncertainties in the streamwise and radial component decrease and increase, respectively with intersection angle. As can be seen from figure 8 (a) and (b) angles between 30-50° offer an ideal balance of uncertainties for this system. The slight linear slope in the bias uncertainty of the azimuthal component is due to changes in transmission with changing intersection angle being dominant.

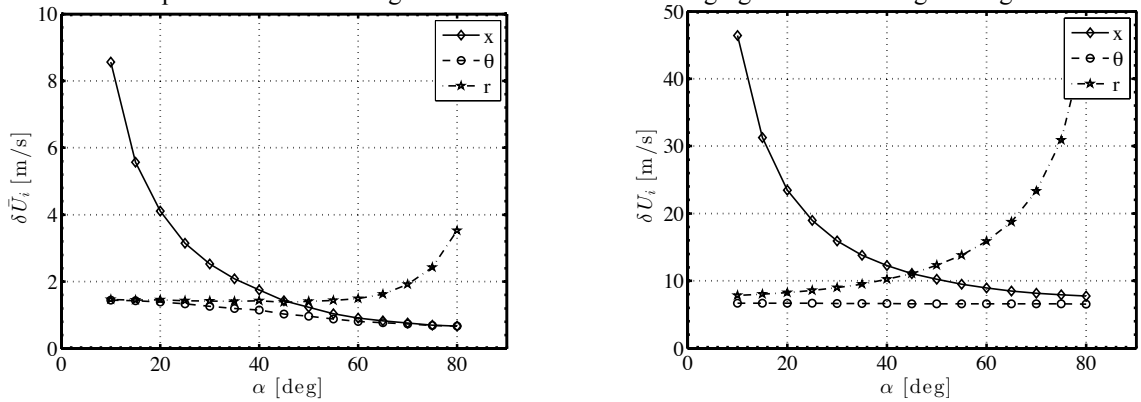

Fig. 8 Bias (a) an instantaneous (b) velocity uncertainty for example case (α is defined in figure 3).

3.4 Laser stability

According to the Springer Handbook of Experimental Fluid Mechanics (Tropea et al. 2007) the laser bandwidth for a successful DGV measurement needs to be smaller than 10 MHz. The Verdi V6 laser used in this study has a line width of about 5 MHz over 20 ms according to Coherent (Coherent Inc. white paper). The line width narrows if observed over smaller times scales such as implemented with the pDV sensor developed here. The reference photodiodes were sampled at 50 MHz during all measurements, therefore minimizing the influence of laser jitter and laser drift on the measurement.

3.5 Transmission line bandwidth limitations

Another critical component of a successful DGV/pDV measurement is the choice of absorption line. For low flow speed application the sensitivity to velocity change is the main concern as it directly influences the physical uncertainties. However for high-speed application with extreme Doppler shifts the line bandwidth compared to the Doppler bandwidth is most essential. Even when the mean velocity shift is placing the measured transmissions on the center of an absorption line, the turbulent motion of the fluid can cause an extreme standard deviation from the mean shift.

In figure 9 an example case with large frequency shifts is displayed. It can be seen from the figure that there are non-unique regions bounding the line bandwidth to about 720 MHz (representative of half bandwidth of line 89.95 1/cm, compare to figure 2). In these cases of large Doppler shifts and large standard deviations, this limitation can clip and distort the measured velocity statistics compared to the true values.

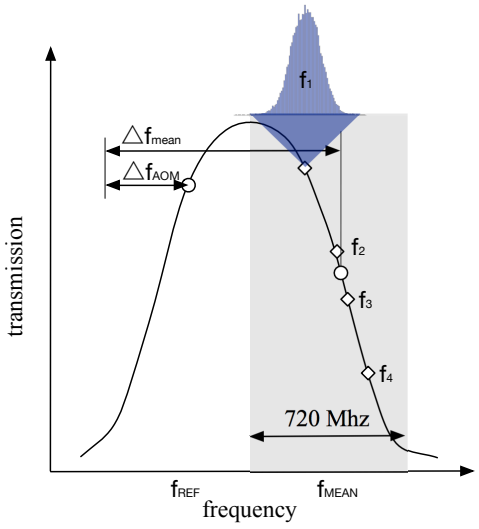

Fig. 9 Transmission line bandwidth limitations for turbulent flows

The total bandwidth necessary is determined from the difference of the highest and lowest frequency of the frequencies to be measured. As for this particular technique, four possible frequency combinations exist; the lowest possible bandwidth is then defined by the lowest bandwidth of one of the possible combinations of f_1,f_2,f_3 and f_4. Measurements that have a lower required bandwidth than the measurement line width can still be subject to bounding as the distribution of frequencies (indicated by a Gaussian histogram in figure 9) come close to the bounding sides of the line.

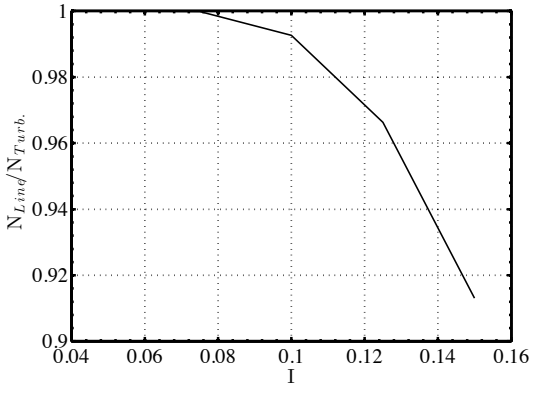

Fig. 10 Line coverage decreasing with increasing turbulent intensity due to clipping, for example case

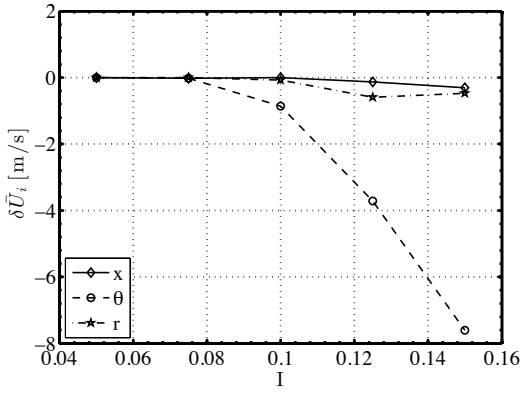

Fig. 11 Mean velocity error due to line bounding at high turbulent intensity, for example case

Figure 10 shows the line coverage for synthetic datasets with increasing turbulent intensities (f_{AOM}=-80 MHz, α=45°). For a center frequency (f_{mean}) fixed on the center of the line flank, increasing turbulent intensity leads to clipping – frequencies that are not covered by the bandwidth of the transfer function. Line coverage is here defined as the number of observable data points N_{Line} on a real transmission line divided by the number of observable data points $N_{Turb.}$ on an idealized transmission line. The center of

the frequency shift can be shifted relative to the reference frequency f_{REF} by using an AOM, this shift is denoted by f_{AOM} in figure 9.

For this example case with relatively high mean velocities and turbulent intensities of 15%, up to 9% of the dataset cannot be observed due to bandwidth limitations. Figure 11 shows the absolute error (bias) of the mean velocity for the example case. Individual instantaneous measurements as discussed in the previous section are not affected with a bandwidth-induced error since measurements exceeding the bandwidth are invalid, with no means for estimating velocity. However, statistics and spectral information will obviously be impacted due to bandwidth limits. For measurements of highly turbulent flows with high mean velocities these physical limitations need to be observed in order to allow accurate measurements of velocity statistics. As the presented results are for a system with 532 nm laser wavelength, the use of a laser with higher wavelength, e.g. 852.3 nm as used by Fischer et al. (2007) would significantly decrease the required Doppler frequency bandwidth and increase the effective dynamic range of the instrument.

4. Implementation: Apparatus and instrumentation

The interest driving the instrument development is the need to understand the production of noise in supersonic jets. Lighthill(1952) made a first theoretical approach to jet noise in 1952 with his famed acoustic analogy, representing the fluctuations of the local flow by a distribution of quadrupole sources with equivalent energy. This analogy is strongly dependent on the source terms described by the Lighthill stress tensor (Tam 1995) which can be deduced from higher order correlations. To further physical understanding of the noise generation processes and to enable validation of numerical models, time-accurate measurements of supersonic jets are therefore inevitable.

4.1 Facility

The Virginia Tech hot jet facility has been described in past works (Ecker et al. 2014b; Brooks et al. 2014a). This facility provides supersonic flow at TTRs up to 3 at 0.12kg/s mass flow rate. The air is heated by an electrical 192 kW power inline heater. The biconical nozzle used (M_d =1.65; nozzle diameter, d=0.75 in) was adapted from the geometry studied by Powers and McLaughlin (2012) for military-style nozzles, differing in the present study by being axisymmetric and unfaceted.

For the cold flow studied, flow seeding is performed by introducing Di-Ethyl-Hexyl-Sebacat (DEHS) oil droplets generated by a LaVision four-nozzle flow seeder unit. This unit is capable of generating sub-micron droplet sizes, and particle response time can be estimated for a 1 µm diameter particle from Stokes drag (Ecker et al. 2012) assuming continuum regime flow, to be about 3.8 µs at a flow static temperature of 200 K.

4.2 Instrument configuration and properties

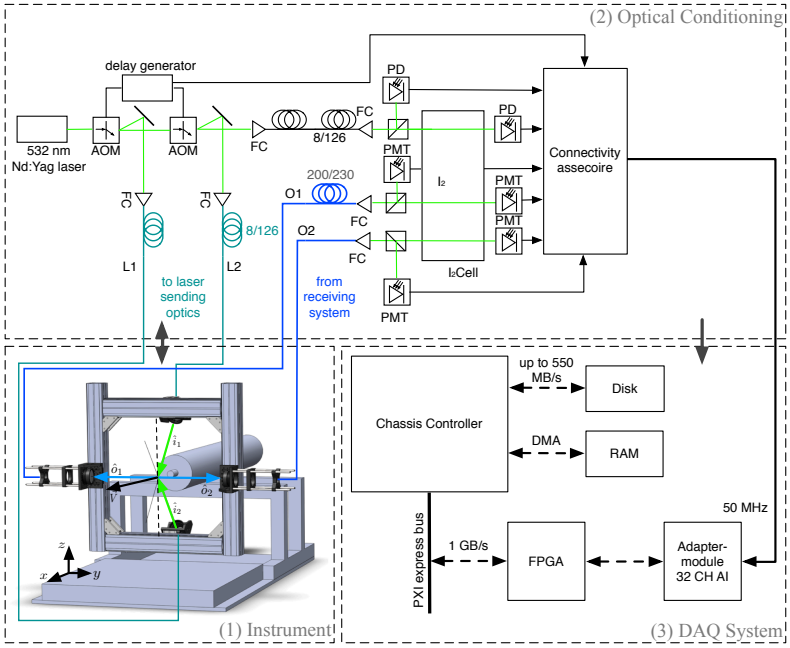

Fig. 12 Optical layout of pDV probe (FC: beam to fiber coupler, AOM: Acousto Optic Modulator, PD: Photodiode, PMT: Photomultiplier tube)

Figure 12 shows the optical setup for the described pDV system. Essential system parameters are tabulated in table 3. The setup can be separated into three different zones: (1) instrument, (2) optical conditioning and (3) data acquisition. The instrument here refers to the device that is attached to the facility and generates the measurement volume as well as collects the scattered light. The measurement volume created by the 250 mm focal length sending lens is estimated to be about 60 μm diameter. The two laser heads are consecutively flashing to generate two velocity components at a time. The receiving optics (f=200 mm) focuses the received light into 200 μm telecommunication grade multimode fiber.

Optical conditioning is performed on a separate optical table in an adjacent room. Multiplexing is enabled by using two 80 MHz AOMs produced by Intraaction Corp. as optical switches, turning on and off the respective beam. A BNC 565 signal delay generator controls the multiplexing time interval, which is the interval each beam consecutively activates. The laser beam is shifted by -80 MHz and then transmitted to the instrument by an 8 μm core diameter telecommunication grade multimode fiber. PMT and photodiode (PD) calibration measurements are performed before every experimental section. As this calibration is performed in-situ all errors due to alignment, beamsplitting cubes imperfection and polarization dependencies are taken into account to the greatest extent possible. Two photodiodes (Thorlabs PDA100A) are used to monitor the unshifted laser frequency through the iodine gas cell at all times, reducing the influence of laser frequency drift or fluctuation to a minimum. Four Hamamatsu R4124 PMTs are used for transducing the received Doppler shifted photons into voltage signals.

Tab. 3 Instrument parameters

Parameters	
Measurement volume beam waist diameter	60 μs
Laser power (per beam)	160 mW
Multiplexing time-step	2 μs
α	45 °
Sampling rate DAQ	50 MS/s
Iodine cell body temperature	60°C

The experimental data are acquired by a NI PXIe DAQ system using a 50 Mega Samples/S (MS/s) Adapter-module (NI 5752) on a FlexRIO FPGA (NI PXIe-7965R) unit. All four PMTs signals, as well as the PD signals and the AOM switching signals are recorded simultaneously at 50 MS/s. Datasets were typically 50 Million samples, which equals to 1 sec. in duration. Tuning the cavity length inside the Coherent Verdi V6 CW Diode-Pumped Solid-State Laser is performed by controlling a piezoelectric element (PZT) inside the laser, using a 0-72 V BK Precision bench-top power supply. This allows choosing the transmission line at which the sensitivity and bandwidth of the transfer function is optimal.

4.3 In situ uncertainties

Tab. 4 Associated uncertainties for example case

Systematic uncertainties			
	$\delta\overline{U}_x$ [m/s]	$\delta\overline{U}_\theta$ [m/s]	$\delta\overline{U}_r$ [m/s]
Processing error	0.042	0.975	0.128
Instrument uncertainty	1.420	1.025	1.362
Geometrical uncertainty	0.597	0.443	0.572
Total uncertainty	**1.541**	**1.482**	**1.483**
Instantaneous uncertainties			
	δU_x [m/s]	δU_θ [m/s]	δU_r [m/s]
Processing error	6.175	1.120	6.195
Instrument uncertainty	9.200	6.508	9.190
Geometrical uncertainty	0.597	0.443	0.572
Total uncertainty	**11.10**	**6.618**	**11.10**

From the previous analysis the uncertainty in each measured component can be determined for a 45° angle configuration for an example case ([500,30,20] m/s, I=0.15 Δt = 2 μs, 50,000 samples and SNR 20dB signal, misalignment of geometry by 0.14 deg). Table 4 (top) shows the associated systematic uncertainties. Table 4 (bottom) gives the specific uncertainties for the case of the time-resolved instantaneous measurements. The relative uncertainties are excellent for the streamwise component but somewhat higher for radial and azimuthal components. Different geometrical arrangements and multiplex time-steps can be

used to decrease the uncertainty in those components. For comparison, Thurow et al.(2005) give a velocity error for their 1-component camera based system of about 9-33m/s for measurements in their Mach 2.0 supersonic jet. Fischer et al. (2013) reported a measured uncertainty of about 1 m/s at 100 kHz laser modulation frequency for their laboratory scale experiments.

In the following section, instrument performance is validated with a LDV probe with measurements in in a cold supersonic jet, and an exposition of the instrument time response is provided via measurements of Reynolds stress spectra stream-wise development.

5. Results and discussion

In order to evaluate the pDV instrument performance, measurements at different jet NPR at the same location were performed repeatedly. These measurements are then compared to a 2-component LDV measurement at the same location. Details on the LDV probe used can be found in Brooks et al. (2014a,b). The instantaneous uncertainty of the LDV measurements is 0.33% of the measured velocity, with systematic uncertainty in the fringe spacing of the same order. Uncertainties of the pDV probe are given in table 4, with approximately the same magnitude for bias errors as the LDV. The horizontal error bars in figure 13 are determined from the uncertainties in the NPR value due to uncertainties in the reference pressure and total pressure readings and explain small discrepancies between LDV and pDV measurement over the instrumentation uncertainties themselves. The comparison of the mean velocity data in figure 13 shows excellent agreement within positioning, pressure and velocity uncertainties. Measurements were repeatable and consistent over the course of the experiment.

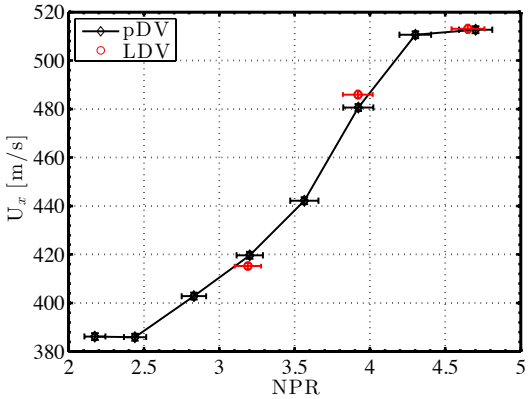

Fig. 13 mean velocity measurement at a static position in the jet

After validation of the pDV probe, measurements along the streamwise axis at a normalized radial coordinate of r/d=0.2 and NPR=3.2 (T_0=300K; isentropic Mach number, M_j=1.4) are performed. At this condition the jet is highly over-expanded and exhibits the screech phenomenon. The measurement volume moves through several normal and oblique shocks as well as expansion waves before it enters a region where the potential core breaks down and large and small scale turbulent mixing occurs. Mean data rates of up to 100 kHz were reached in the potential core where particle seeding was optimal. Local data rates were up to 250 kHz over periods of time, but could not be sustained due to the Poisson statistics of particle arrival resulting in periods of data dropout.

Mean stream-wise, radial and azimuthal velocities along the stream-wise coordinate are displayed in figure 14. It is to note that the streamwise and radial velocities clearly reflect the shock-cell structure in the potential core as well as the break down further downstream.

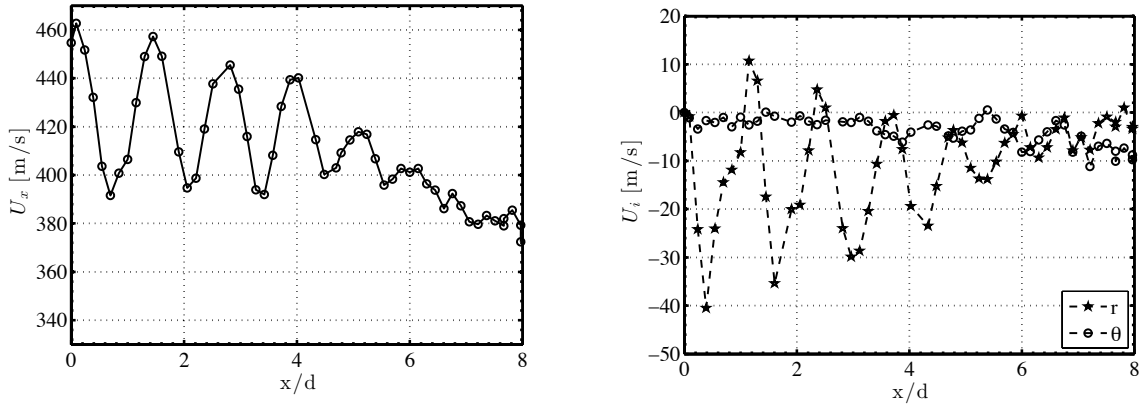

Fig. 14 Mean streamwise (a) and radial and azimuthal (b) velocities along the streamwise coordinate (NPR=3.2,M_j=1.4, TTR=1, r/d=0.2)

From this measurement it appears that there are four strong shock cells in the mean at this condition. This is consistent with Schlieren photographs from this region. The azimuthal velocity does not

show this behavior. The velocity vectors were rotated using the information at the exit plane to have zero radial and azimuthal velocity. The drift in the mean azimuthal velocity is most likely due to precession of the shock structure; at 7.8kHz it would only require a precession radius of 1.3 mm to obtain this effect.

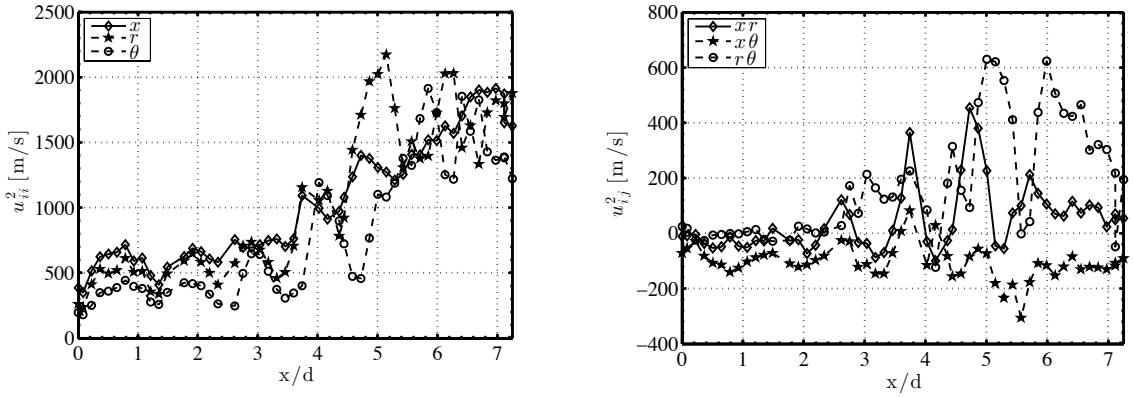

Fig. 15 Normal (a) and shear (b) stresses along the streamwise coordinate (NPR=3.2,M_j=1.4, TTR=1, r/d=0.2)

After a distance x/d larger than 4, a strong rise of the Reynolds normal stresses due to shock unsteadiness growth and flow instability can be observed. This trend is displayed for all normal stresses in figure 15 a. At 5 diameters the streamwise normal stresses correspond to a turbulence intensity of about 0.12. A similar trend and magnitude was shown by Alkislar and Krothanalli (2003) for the streamwise normal and transverse stresses in a rectangular under-expanded supersonic jet, as well as by Lau et al. (1979) and Bridges and Wernet (2008) for normal stresses in axisymmetric fully expanded supersonic jets. Alkislar and Krothapalli's data also showed a peak in the transverse mean Reynolds stress that peaked above the magnitude of the streamwise normal stresses before dropping to lower values, similar to the radial normal stress displayed in figure 15 a.

A fuzzy slot correlation technique (Benedict et al. 2000) allows to obtain auto and cross-correlation from the non-equally spaced velocity data. The Wiener-Khinchin theorem grants direct conversion of the auto and cross-correlation into auto and cross-spectra.

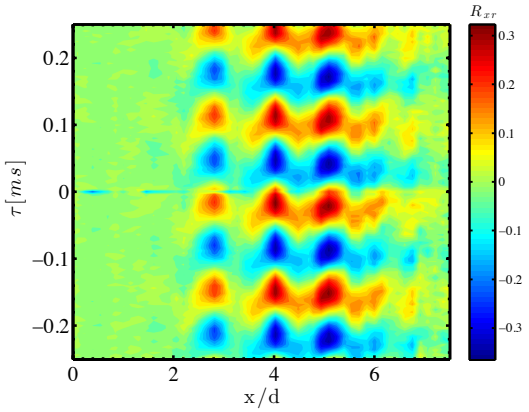

Fig. 16 Cross-correlation of the stream wise and radial velocity along the streamwise coordinate (NPR=3.2, M_j=1.4, TTR=1, r/d=0.2)

The behavior of shock unsteadiness, or screech, is examined in the spectral and time-delay domains. As first proposed by Powell (1953), axisymmetric, helical and lateral modes of screech are possible. As verified using Schlieren photography, the jet under study exhibited the helical instability mode. In figure 16, the development of the Reynolds shear stress time-delay cross-correlation is exhibited. While the findings from the visualizations of Umeda and Ishii (2001) indicate that the helical mode initiated in the third shock cell for the under-expanded jets they studied, the current results for the over-expanded jet indicate significant strength of the fundamental screech tone in the shear stress just upstream of the third shock, shifted toward the nozzle exit by ½ a cell compared with the under-expanded jet. The rapid decay of the fundamental tone three shock cells downstream of its appearance is in contrast to the recent results of Edgington-Mitchell et al. (2014) for under-expanded jets, as well. The authors there indicate a strong persistence of the fundamental helical mode signature out to x/d = 9. Time-accurate Schlieren videos obtained for the jet currently under study indicated a violent screech mode that likely grew into a non-linear regime causing its rapid breakdown. Another interesting aspect of the time-delay data is the variable phase shift between the stream-wise and radial fluctuation velocities with stream-wise distance, particularly visible in the three shock cells with clear fundamental mode content, between 3 and 5 diameters. These shifts occur in the regions of high

stream-wise velocity gradients, with increasing phase shift magnitude between stream-wise and radial velocity fluctuations in shock regions and decreasing phase shift magnitudes in the expansion regions. Again from the Schlieren images, it appears that this variable phase is due to the lag between the helical motion of the jet core and the formation of the shock. The visualization indicates a highly unsteady shock at x/d = 3, contributing the mechanism for this phase lag.

Spectral analysis of the Reynolds stresses measured reveals the loci of fundamental and harmonic screech tone dominance (compare figure 17). The stream-wise normal stress results generally follow the behavior deduced from the time-delay correlation results - the fundamental screech tone is shown to dramatically diminish for x/d > 6. However, interestingly, the radial/azimuthal shear stress exhibits significant content from the screech tone throughout the measurement range. It is likely that this difference is explainable due to the appearance of vortical turbulence due to the penetration of the shear layer into the potential core. For the stream-wise normal stress, contributions from turbulence produced by axisymmetric shear are significant and may swamp out the screech signal. However, there are no mechanisms for production of radial-azimuthal shear stress in the axisymmetric jet beyond the screech instability itself. Thus we would expect that production of that shear stress would be intrinsically linked to the spectral content of the screech mechanism, causing the strong persistence of this signature in the shear stress spectra, as seen in figure 17.

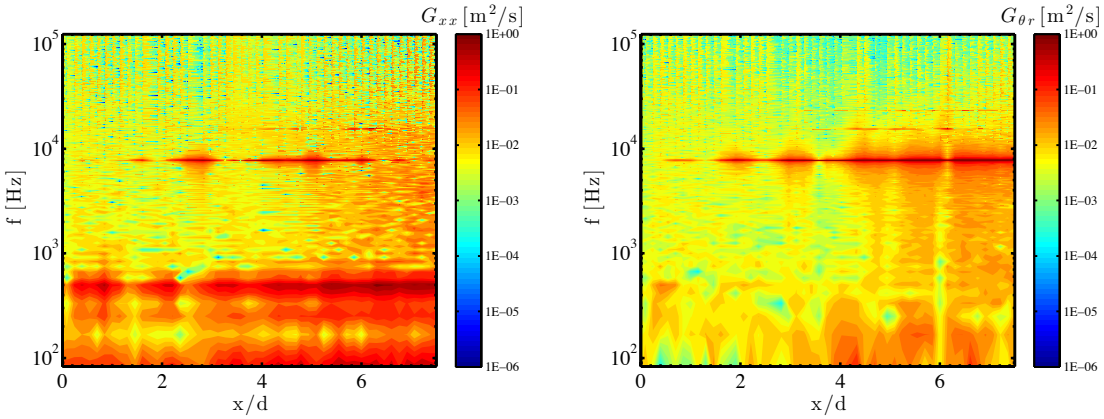

Fig. 17 Streamwise velocity auto (a) and radial-azimuthal velocity cross-spectra (b) along the streamwise coordinate (NPR=3.2,M_j=1.4, TTR=1, r/d=0.2)

6. Conclusions

A new probe making use of the DGV technique has been developed and is presented in the framework of state of the art development of DGV technology. Especially the time shift multiplexing is a new approach reducing required sensor devices while still enabling the time response capable of high speed flow applications.

In a study on the data processing and its induced errors it was found that next to the geometric configuration the flow timescales are of largest impact. Reducing the time-shift period allows reducing associated errors significantly. For timescales relevant to the jet noise application, the instantaneous velocity errors due to processing are about 6.1 m/s for streamwise and radial component and around 1.0 m/s for the azimuthal velocity component for the example case with timescales of interest as low as 10 µs.

The detailed heuristic uncertainty analysis propagates the uncertainties of the linearized DGV transfer function and allows obtaining a reasonable estimate of the measurement uncertainties. Results from the processing analysis were included and the total measurement uncertainty expressed as a root square sum of the uncorrelated contributions of data processing errors and physical uncertainties. The uncertainties for the presented instrument are about 1.5 m/s for mean measurements and between 6.6 and 11.1 m/s for instantaneous measurement of the 3-component velocity vector.

It is shown that using velocity multiplexing is an effective method to reduce instrument cost without sacrificing mean uncertainties. Uncertainties for the instantaneous velocity vectors are mainly characterized by random effects such as signal to noise ratio as well as temporal averaging effects. Achieved uncertainties compare favorable to previous work in time-resolved DGV. Implications of the transmission line width for measurement of flows with high mean velocities and high turbulent intensities are discussed and examples for associated uncertainties given. Using a different laser with a higher

wavelength could compress the required transfer function bandwidth and increase the dynamic range of the instrument therefore eliminating these physical limitations.

First measurements in a supersonic cold over-expanded jet using a pDV instrument have been performed and the temporal capabilities demonstrated. Mean flow velocity measurements at different tunnel operating pressures have been validated by using a LDV and are within the expected uncertainty range for reference based DGV. By traversing the instrument along the streamwise axis mean flow and full Reynolds stress tensors were obtained. Global data rates of above 100 kHz with local data rates as high as 250 kHz allowed spectral analysis of the Reynolds stress tensors in the streamwise development.

In combination with time-accurate Schlieren videos the current study exposes helical screech modes with a spatial extension fundamentally different from the structures at under-expanded conditions found in literature. Compared to under-expanded conditions the present study shows rapid breakdown due to shock unsteadiness and vortical non-linear instability growth The screech tone phenomenon and its higher harmonics present in the potential core and in regions of increased turbulent mixing and is suspected to be linked to the production of radial-azimuthal shear stresses in extended regions beyond the potential core. While the influence of the screech phenomenon onto the normal stresses quickly diminishes at x/d>6, the signature of the screech remains imprinted onto the radial-azimuthal shear stresses beyond the region of investigation.

This measurement provides insight into the usefulness of time-resolved DGV for understanding dominant turbulent structures for noise generation in supersonic jet flow and highlights the need for ongoing development of time-resolved multi-point measurements. This study discusses in detail a geometrical configuration that can be easily extended to allow planar and tomographic operation by using spatially resolving sensors, large aperture lens systems and scanning laser sheets.

Acknowledgements

The work described was supported by the Office of Naval Research Hot Jet Noise Reduction Basic Research Challenge and DURIP, grants N00014-11-1-0754 and N00014-12-1-0803 under program managers Drs. Brenda Henderson and Joseph Doychak.

References

Alkislar M. B., Krothapalli A., & Lourenco L. M. (2003). Structure of a screeching rectangular jet: a stereoscopic particle image velocimetry study. *Journal of Fluid Mechanics*, *489*, 121-154.

Benedict L. H., Nobach H., & Tropea C. (2000). Estimation of turbulent velocity spectra from laser Doppler data. *Measurement Science and Technology*, *11*(8), 1089.

Bridges J. E., & Wernet M. P. (2008). Turbulence associated with broadband shock noise in hot jets. NASA/TM-2008-215274,

Brooks D.R., Ecker T., Lowe K.T., Ng W.F. (2014a) Experimental Reynolds Stress Spectra in Hot Supersonic Round Jets. *AIAA SciTech (52nd Aerospace Sciences Meeting)*.

Brooks D.R., Lowe K.T. (2014b) Fluctuating Flow Acceleration in a Heated Supersonic Jet. In *Proc. 17th Int. Symp. on Applications of Laser Techniques to Fluid Mechanics (Lisbon, Portugal, 7–10 July)*.

Cadel D. R., Ecker T., & Lowe K. T. (2014a). Time-Domain Cross-Correlation Scan DGV (CCS-DGV) for Mean-Velocity Boundary Layer Measurements. *AIAA SciTech (52nd Aerospace Sciences Meeting)*.

Cadel D. R., Ecker T., & Lowe K. T. (2014b). Volumetric vector velocity measurements in a hot supersonic jet. In *Proc. 17th Int. Symp. on Applications of Laser Techniques to Fluid Mechanics (Lisbon, Portugal, 7–10 July)*.

Cavone A. A., Meyers J. F., & Lee J. W. (2006) Development of point Doppler velocimetry for flow field investigations. In *Proc. 13th Int. Symp. on Applications of Laser Techniques to Fluid Mechanics (Lisbon, Portugal, 26–29 June)*.

Chan VSS., Heyes A. L., Robinson D. I., & Turner J. T. (1995) Iodine absorption filters for Doppler global velocimetry. *Measurement Science and Technology, 6(6)*, 784–794

Charrett T.O.H., Ford H.D., Nobes D.S., Tatam R.P. (2004) Two-frequency planar Doppler velocimetry (2v-PDV). *Review of Scientific Instruments* 75:4487–4496.

Charrett T. O. H., Nobes D. S., & Tatam R. P. (2007). Investigation into the selection of viewing configurations for three-component planar Doppler velocimetry measurements. *Applied optics*, *46*(19), 4102-4116.

Coherent Inc. white paper, Wavelength Control and Locking with Sub-MHz Precision

Clancy P.S., Samimy M., and Erskine W.R. (1999) Planar Doppler Velocimetry: Three-Component

Velocimetry in Supersonic Jets. *AIAA Journal 37:6*, 700-707
Ecker T., Lowe K.T., Ng W.F., and Brooks D.R. (2014a) Fourth-order Spectral Statistics in the Developing Shear Layers of Hot Supersonic Jets. *Propulsion and Power (50th AIAA/ASME/SAE/ASEE Joint Propulsion Conference)*
Ecker T., Brooks D.R., Lowe K.T., Ng W.F. (2014b). Spectral analysis of over-expanded cold jets via 3-component point Doppler velocimetry. *AIAA Scitech (52nd Aerospace Sciences Meeting)*
Ecker T., Lowe K.T., Simpson R.L. (2012). Novel Laser Doppler Acceleration Measurements of Particle Lag through a Shock Wave. *50th AIAA Aerospace Sciences Meeting including the New Horizons Forum and Aerospace Exposition*
Edgington-Mitchell D., Oberleithner K., Honnery D. R., & Soria J. (2014). Coherent structure and sound production in the helical mode of a screeching axisymmetric jet. *Journal of Fluid Mechanics,* 748, 822-847.
Elliott G. S., & Beutner T. J. (1999). Molecular filter based planar Doppler velocimetry. *Progress in Aerospace Sciences, 35(8)*, 799–845.
Fischer A., Büttner L., Czarske J. (2011) Simultaneous measurements of multiple flow velocity components using frequency modulated lasers and a single molecular absorption cell. *Optics Communications* 284:3060–3064. doi: 10.1016/j.optcom.2011.02.070
Fischer A., Büttner L., Czarske J., Eggert M., Grosche G., & Müller H. (2007). Investigation of time-resolved single detector Doppler global velocimetry using sinusoidal laser frequency modulation. *Measurement Science and Technology, 18(8)*, 2529–2545.
Fischer A., Büttner L., Czarske J., Eggert M., & Müller H. (2008). Measurement uncertainty and temporal resolution of Doppler global velocimetry using laser frequency modulation. A*pplied Optics, 47(21)*, 3941–3953
Fischer A., Pfister T., Czarske J. (2010) Derivation and comparison of fundamental uncertainty limits for laser-two-focus velocimetry, laser Doppler anemometry and Doppler global velocimetry. *Measurement* 43:1556–1574.
Fischer M., Heinze J., Matthias K., & Röhle I. (2000, July). Doppler global velocimetry in flames using a newly developed, frequency stabilized, tunable, long pulse Nd: YAG laser. In *Proc. 10th Int. Symp. on Applications of Laser Techniques to Fluid Mechanics (Lisbon, Portugal, 10–13 July)*.
Fischer A., König J., Haufe D., Schlüßler R., Büttner L., & Czarske J. (2013). Optical multi-point measurements of the acoustic particle velocity with frequency modulated Doppler global velocimetry. *The Journal of the Acoustical Society of America*, *134*(2), 1102-1111.
Forkey JN (1996) Development and Demonstration of Filtered Rayleigh Scattering: a Laser Based Flow Diagnostic for Planar Measurement of Velocity, Temperature and Pressure.
Forkey JN, Lempert WR, Miles RB (1997) Corrected and calibrated I_2 absorption model at frequency-doubled Nd:YAG laser wavelengths. *Appl Opt, AO* 36:6729–6738.
Freund J. B., Lele S. K., Moin P. (2000). Compressibility effects in a turbulent annular mixing layer. Part 1. Turbulence and growth rate. *Journal of Fluid Mechanics*, 421, 229–267.
Fussell J (2003) Refinement and Verification of the Virginia Tech Doppler Global Velocimeter (DGV).
Jones T (2001) Development and Testing of the Virginia Tech Doppler Global Velocimeter (DGV).
Komine H. (1990). *U.S. Patent No. 4,919,536*. Washington, DC: U.S. Patent and Trademark Office.
Komine H., Brosnan S.J., Litton A.B., Stappaerts E.A. (1991) Real-time, Doppler global velocimetry. *29h AIAA Aerospace Sciences Meeting.*
Kuhlman J., Collins P., & Scarberry T. (2001). Two-component point Doppler velocimetry data in circular jets. *Measurement Science and Technology, 12(4)*, 395–408.
Lau J.C., Morris P.J., Fisher M.J. (1979) Measurements in subsonic and supersonic free jets using a laser velocimeter. *Journal of Fluid Mechanics.* 93:1–27.
Lighthill M.J. (1952) On Sound Generated Aerodynamically. I. General Theory. *Proceedings of the Royal Society A: Mathematical, Physical and Engineering Sciences* 211:564–587.
Lowe K. T., Ng W. F., & Ecker T. (2012). Early Development of Time-Resolved Volumetric Doppler Velocimetry for New Insights in Hot Supersonic Jet Noise. 18th AIAA/CEAS Aeroacoustics Conference (33rd AIAA Aeroacoustics Conference)
Meyers J., Lee J. (2010) Boundary layer measurements in a supersonic wind tunnel using Doppler global velocimetry. *Proc. 15th Int. Symp. on Applications of Laser Techniques to Fluid Mechanics (Lisbon,*

Portugal, 05–08 July)
Meyers J. F., & Komine H. (1991). Doppler global velocimetry: a new way to look at velocity. *Laser Anemometry*, *1*, 289-296.
Meyers J.F., Lee J.W., Schwartz RJ (2001) Characterization of measurement error sources in Doppler global velocimetry. *Measurement Science and Technology* 12:357–368.
Müller H., Lehmacher T., & Grosche G. (1999). Profile sensor based on Doppler global velocimetry. In *8th International conference laser anemometry advances and applications* (pp. 475-482).
Nobes D. S., Ford H. D., & Tatam R. P. (2004). Instantaneous, three-component planar Doppler velocimetry using imaging fibre bundles. *Experiments in Fluids, 36(1)*, 3–10.
Pope S.B. (2000) Turbulent Flows - Cambridge University Press
Powell A. (1953). On the mechanism of choked jet noise. *Proceedings of the Physical Society. Section B*, *66*(12), 1039.
Powers R. W., & McLaughlin D. K. (2012). Acoustic measurements of scale models of military style supersonic beveled nozzle jets with interior corrugations. *AIAA Paper*, *2116*, 18th AIAA/CEAS Aeroacoustics Conference (33rd AIAA Aeroacoustics Conference)
Reinath M.S. (1997). Doppler Global Velocimeter Development for the Large Wind Tunnels at Ames Research Center. NASA TM 112210
Smith M. W. (1998). Application of a Planar Doppler Velocimetry System to a High Reynolds Number Compressible Jet, Presented at the 36th AIAA Aerospace Sciences Meeting and Exhibit, Reno, NV
Tam C. K. (1995). Supersonic jet noise. *Annual Review of Fluid Mechanics*, *27*(1), 17-43.
Thurow B. S., Jiang N., Lempert W. R., & Samimy M. (2005a). Development of megahertz-rate planar Doppler velocimetry for high speed flows. *AIAA journal*, *43*(3), 500-511.
Thurow B. S., & Lynch K. P. (2009). Development of a high-speed three-dimensional flow visualization technique. AIAA journal, 47(12), 2857-2865.
Tropea C., Yarin A. L., & Foss J. F. (Eds.). (2007). Springer handbook of experimental fluid mechanics (Vol. 1). Springer.
Umeda Y., & Ishii R. (2001). On the sound sources of screech tones radiated from choked circular jets. *The Journal of the Acoustical Society of America*, *110*(4), 1845-1858.
Wernet M. P. (2007). Temporally resolved PIV for space–time correlations in both cold and hot jet flows. *Measurement Science and Technology*, *18*(5), 1387.